Unraveling Non-Equilibrium Generation of Atomic Nitrogen and Hydrogen in Plasma Aided Ammonia Synthesis

Ning Liu[a], Xingqian Mao[a*], Christopher Kondratowicz[a], Timothy Y. Chen[a,#], Bowen Mei[a], Ziyu Wang[a], Yijie Xu[a], Hongtao Zhong[a,$], Zhiyu Shi[a], Anatoli Morozov[a], Arthur Dogariu[a,b], and Yiguang Ju[a,c]

[a]*Department of Mechanical and Aerospace Engineering, Princeton University, Princeton, NJ 08540, USA*

[b]*Department of Aerospace Engineering, Texas A&M University, College Station, TX 77843, USA*

[c]*Princeton Plasma Physics Laboratory, Princeton, NJ 08540, USA*

*Corresponding author email address: xingqian@princeton.edu

ABSTRACT Non-equilibrium generation of atomic nitrogen and hydrogen governing the ammonia production both in the gas phase and on the catalyst surface is critical to plasma aided ammonia synthesis. Here, this work studies the non-equilibrium generation of atomic nitrogen and hydrogen with a focus on the kinetic role of vibrational energy transfer of hydrogen molecules in plasma aided ammonia synthesis. By combining two-photon absorption laser induced fluorescence

measurements and plasma kinetic modeling, we found that plasma not only generates ammonia but also produces critical H, N and NH radicals via both electron impact and vibrational energy transfer excitations. The vibrational energy transfer from the excited hydrogen $H_2(v=1)$ to higher vibrational levels $H_2(v=2\text{-}3)$ via the V-V exchange ($H_2(v)$-$H_2(v)$) and V-V' exchange ($N_2(v)$-$H_2(v)$) significantly enhances the H and NH production, and then promotes the coupling between N and NH for ammonia synthesis both in the gas phase and on the catalyst surface.

TOC GRAPHICS

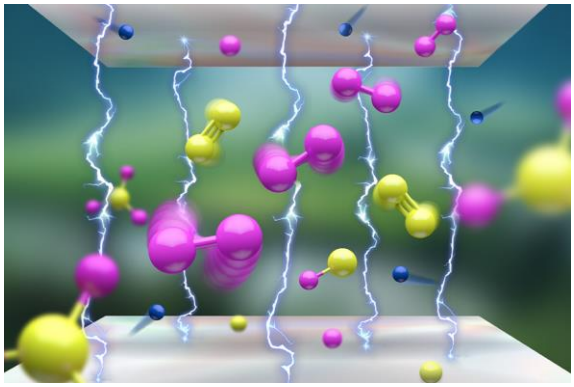

Ammonia (NH_3) represents a key hydrogen (H_2) carrier for sustainable energy and carbon neutrality. It has great potential to be widely applied in power generation[1-2], energy storage[3-4], fertilizer[5-6], and propulsion[7-8]. The traditional way to synthesize NH_3 is the well-known Haber-Bosch process which produces NH_3 with catalyst under high temperature (400 to 650 ^oC) and pressure (200 to 400 atm) conditions[9]. Compared to Haber-Bosch, plasma synthesis has recently

attracted tremendous attention, since it converts renewable electricity to produce NH_3 via non-equilibrium reaction pathways at low temperatures and near atmospheric pressure[10-12]. Plasma aided NH_3 synthesis starts with activation of nitrogen (N_2) and H_2 in the gas phase mainly via electron impact dissociation and excitation, producing energetic N and H radicals as well as electronically and vibrationally excited N_2/H_2. These key radicals and excited species then react either with surface species on the catalyst or directly with other species in the gas phase to produce NH_3[13-14]. Therefore, the generation of atomic N/H and excited species, dictating both surface and gas-phase reaction pathways, is of paramount importance for plasma aided NH_3 synthesis.

However, despite its importance, only a few efforts have been made in understanding the formation of N/H and excited species, and their kinetic roles in producing NH_3. For example, Bayer et al. measured key species (e.g., N/H and $N_2(v)$) and NH_3 using mass spectrometry[15]. Yang et al. explored the plasma-catalytic NH_3 generation mechanism in a nanosecond-pulsed discharge[16]. Wang et al. investigated the effect of catalyst surface on NH_3 formation[17]. Despite these efforts, the underlying chemistry of plasma activation of N_2 and H_2 for NH_3 synthesis is still unclear, especially how N and H radicals are generated and what kinetic role the vibrational-vibrational (V-V/V-V') energy transfer between the same and different vibrationally excited species plays. These pivotal questions have bottlenecked the understanding and development of plasma aided NH_3 synthesis.

With the above discussions, this work aims to understand the non-equilibrium chemistry of plasma N_2 and H_2 activation and unravel the generation mechanism of N and H radicals especially through V-V/V-V' energy transfer in plasma aided NH_3 synthesis. These aims were accomplished by combining quantitative *in-situ* laser diagnostics and plasma kinetic modeling. Figure 1(a) shows the experimental setup of *in-situ* laser diagnostics, i.e., two photon absorption laser induced

fluorescence (TALIF), for detecting H and N radicals in a dielectric barrier discharge (DBD) with an alternating current (AC) power supply. The setup has been detailed elsewhere[18], and here only a brief description is provided. Essentially, this setup consisted of a femtosecond (fs) laser system, an AC-DBD plasma, and an ICCD camera.

The fs laser system (Coherent Vitara-S) as detailed in Ref.[19-21] generated UV fs laser pulses with a pulse energy of 4 μJ at central wavelengths of 205.08 nm for H and 206.65 nm for N and a repetition rate of 1 kHz, by combining a Ti:Sapphire oscillator, an ultrafast amplifier, and an optical parametric amplifier (OPA). The fs laser beam at 205.08 nm (or 206.65 nm) was focused into a rectangular AC-DBD plasma reactor, and to excite the $1s\ ^2S_{1/2} \rightarrow 3d\ ^2D_{3/2,5/2}$ transition of H radical (or the $2p^3\ ^4S_{3/2} \rightarrow 3p\ ^4S_{3/2}$ transition of N radical). The reactor is made of quartz, and it is a plate-to-plate DBD with two thin rectangular stainless-steel electrodes (55 mm × 21 mm) of interelectrode gap 7 mm attached to the outer surface of reactor wall with a thickness of 2 mm. The top electrode was connected to a high voltage AC power supply (PVM500 Plasma Power Generator), and the bottom electrode was grounded. The applied voltage and current waveforms are provided in the Supporting Information. Then, a gas mixture of H_2 and N_2 flowed into this plasma reactor under a pressure of 100 Torr, and the flow rates of H_2 and N_2 were 50 sccm and 450 sccm, respectively. Under the above conditions, micro-discharges randomly distributed between two electrodes as shown in Figure 1(b) were achieved to facilitate the measurements and plasma modeling.

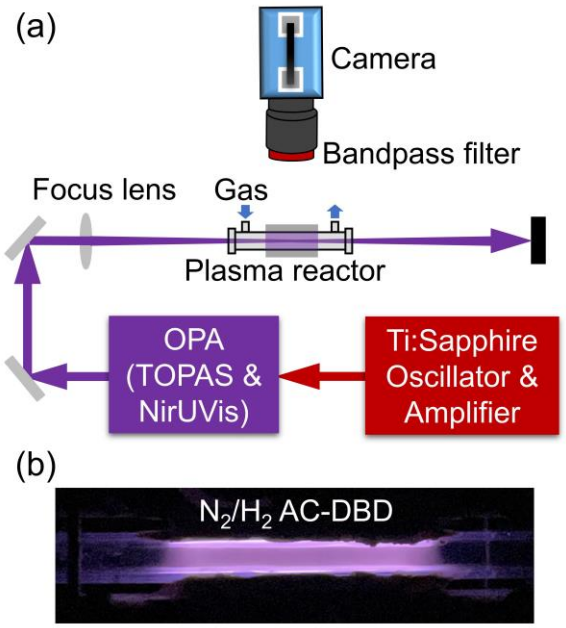

Figure 1 (a) Experimental setup for fs-TALIF and (b) Photo of N_2/H_2 AC-DBD plasma.

The H fluorescence signals emitted at 656.3 nm and the N fluorescence signals at 742-746 nm from the plasma were separately imaged by an ICCD camera (Princeton Instruments PIMAX-4). For H fluorescence, a bandpass filter with a full-width-at-half-magnitude (FWHM) of 10 nm centered at 656 nm was applied in front of the camera lens to block any laser scatter and plasma emissions, while for N fluorescence, a bandpass filter centered at 745 nm with 10 nm FWHM was used. The camera was synchronized with the laser using control electronics, and the gate time was 80 ns. 2000 shots were averaged for each measurement to maintain good signal to noise ratio. To obtain the absolute concentrations of H and N, the H and N fs-TALIF measurements were calibrated using Krypton (Kr) fs-TALIF measurements as detailed in the Supporting Information, since H, N and Kr had similar excitation and fluorescence wavelengths with minor changes[18]. The calibration parameters including cross section, natural lifetime, and quenching rate were taken from Refs.[22-26].

In addition to N and H measurements, we also measured NH_3 concentrations and gas temperature using gas chromatography (GC, Agilent 8890) and Rayleigh scattering, respectively. The gas production containing NH_3 was sampled into the GC equipped with a nitrogen chemiluminescence detector within 5% measurement uncertainty. The gas temperature was measured *in-situ* using Rayleigh scattering as described in the Supporting Information.

Plasma kinetic modeling was performed by a zero-dimensional (0D) hybrid ZDPlasKin-CHEMKIN model[27-28] using a time-splitting scheme[29] to obtain insights into the reaction pathways of N and H. This model used a validated N_2/H_2 plasma chemistry[16, 30-32] to calculate the time evolutions of temperature and various species densities, i.e., vibrationally and electronically excited species, radicals, molecules, ions and electrons, in a plasma discharge. Especially, this N_2/H_2 plasma kinetic model incorporates a comprehensive reaction kinetics of vibrationally excited species involving impact vibrational excitation, vibrational-translational (V-T) relaxation and V-V/V-V' exchange based on Schwartz, Slawsky, and Herzfeld (SSH) theory[33], as well as chemical abstraction reactions based on Fridman-Macheret α-model[34]. The discharge power density was used to calculate the reduced electric field self-consistently in our plasma modeling. To ensure accurate modeling of the Joule heating and heat loss, the measured temperatures were used as inputs in all modeling cases. Detailed descriptions including experimental validation and numerical verification about the plasma kinetic modeling can be found in the Supporting Information.

Figure 2(a)-(d) shows the measurements and model predictions of N, H, NH_3, and temperature at varying plasma voltages and frequencies. Figure 2(a) shows that the N number density increases from 3×10^{13} cm^{-3} to 4×10^{13} cm^{-3}, as the voltage increases from 9 kV (peak to peak) and 18 kV. In addition, an increase in plasma frequency from 20 kHz to 25 kHz results in higher N density,

accurately captured by the kinetic modeling. Similarly, as shown in Figure 2(b), the H number density positively correlated with both voltage and frequency. This correlation is also well captured by modeling. However, the model underestimates the H number density, probably due to the rate constant uncertainties of recombination reactions from H to H_2 at low temperatures. Figure 2(c) shows the NH_3 production at different voltages and frequencies. As seen, the NH_3 production increases from ~ 140 ppm to ~ 420 ppm, as the voltage climbs from 9 kV to 18 kV at 20 kHz with higher energy deposition. At a frequency of 25 kHz, NH_3 remains high, and it increases from ~ 175 ppm to ~ 530 ppm with the voltage increasing from 9 kV to 18 kV. Lastly, Figure 2(d) shows the temperature measurements obtained by *in-situ* Rayleigh scattering. As expected, the temperature rises with a higher energy input and Joule heating at increased voltages and frequencies.

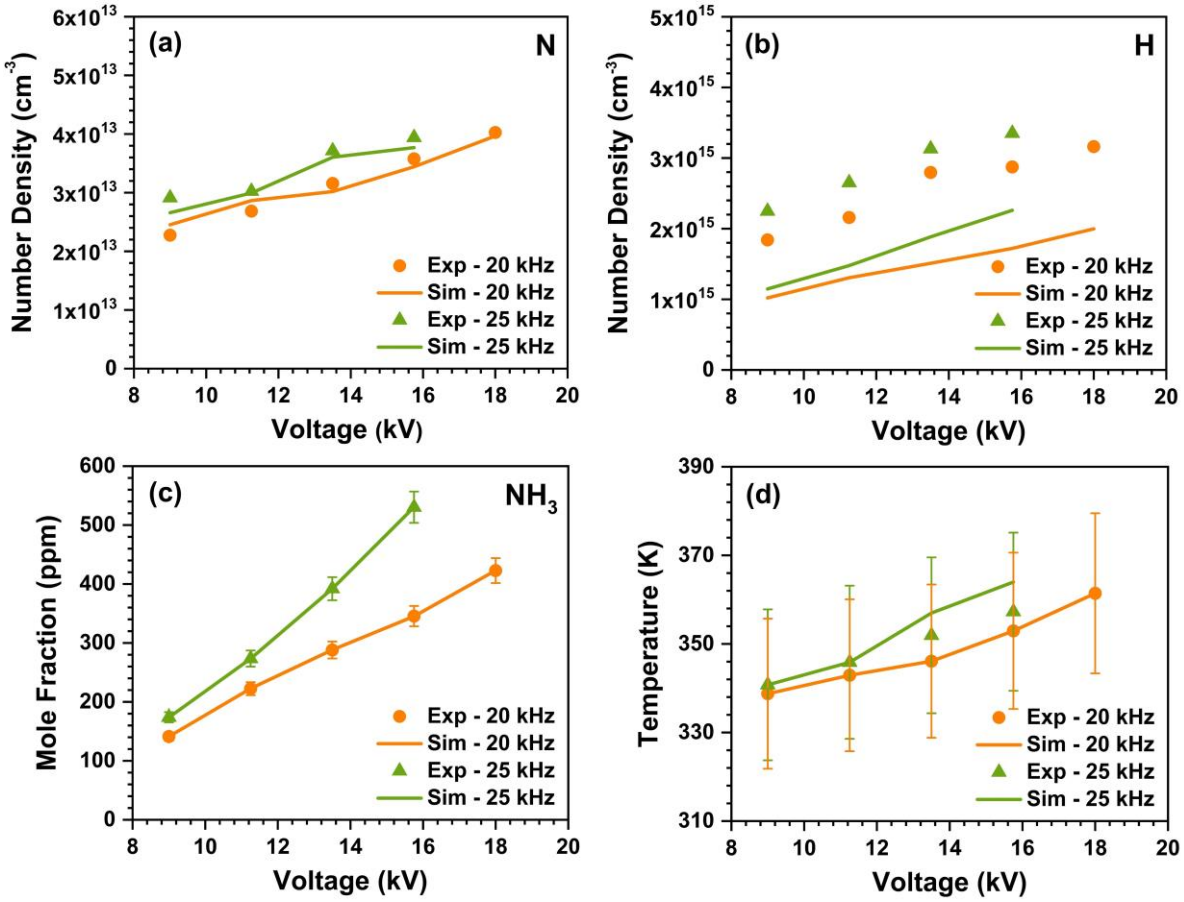

Figure 2 Experimental results and model predictions of (a) N number density, (b) H number density, (c) NH_3 mole fraction and (d) temperature at varying voltages and frequencies in a 0.9 N_2/0.1 H_2 AC plasma discharge.

Based on the above experimental and modeling results, we examined the reaction pathways for N and H radicals as shown in Figure 3, as these radicals are key to the NH_3 production both on the catalyst surface and in the gas phase. In a plasma discharge, N and H radicals are initially produced by direct electron impact dissociation $e + N_2 \rightarrow e + N + N(^2D)$ and $e + H_2 \rightarrow e + H + H$ as well as the collisional quenching of electronically excited nitrogen N_2^* via $N_2(A, a', C) + H_2 \rightarrow N_2 + H + H$. NH_3 is then formed in the gas phase from the H and N radicals via the reaction pathways N

$\xrightarrow{+H(+M)}$ NH $\xrightarrow{+H(+M)}$ NH_2 $\xrightarrow{+H(+M)}$ NH_3. Interestingly, in this work, new plasma reaction pathways involving vibrationally excited $H_2(v)$ and $N_2(v)$ are identified in the micro-discharges at a low reduced electric field region. These reactions affect the N and H production and then NH_3 formation both on the catalyst surface and in the gas phase. Figure 3(b) shows that the high vibrational levels of $H_2(v=2)$ and $H_2(v=3)$ contribute to the NH and H production by inducing new reaction pathways N + $H_2(v=2)$/$H_2(v=3)$ → NH + H, which are also the major N consumption pathways, accounting for 47.3% of N consumption. The process accelerates the aforementioned gas-phase NH_3 formation pathways, and further promotes the coupling between N and NH. This indicates that plasma not only generates NH_3 by itself, but also prepares key H, N and NH radicals via electron impact and vibrational energy transfer for adsorption onto the catalyst surface and NH_3 synthesis reactions thereon. Figure 3(a) also shows that the first vibrational level $N_2(v=1)$ contributes to the NNH production via $N_2(v=1)$ + H → NNH. However, NNH quickly decomposes into N_2 and H, and thus negligibly affects the H concentration.

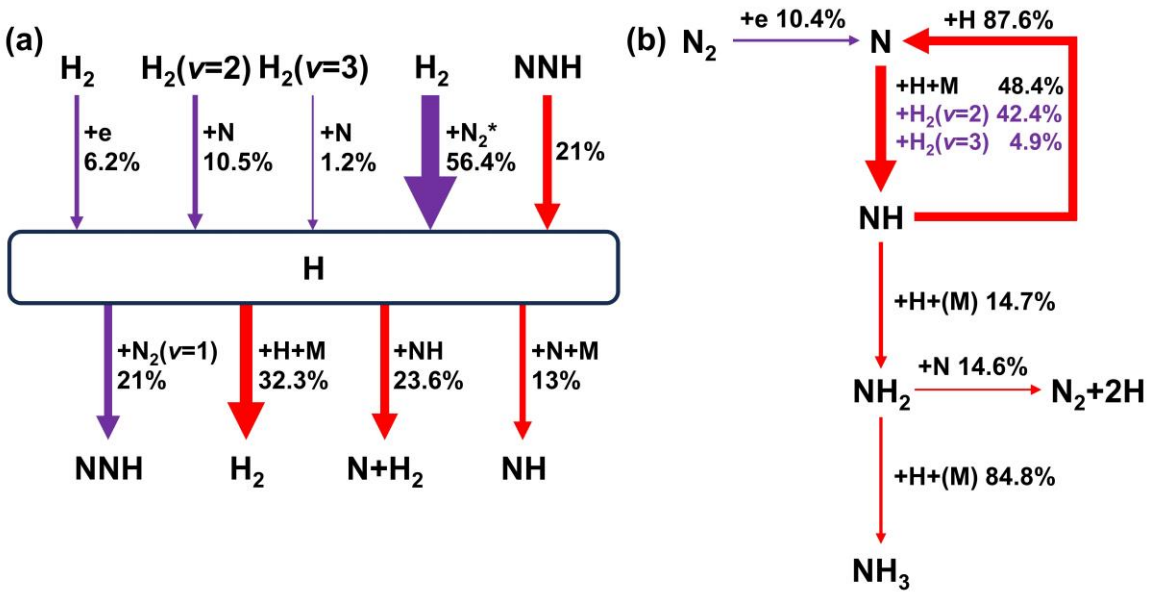

Figure 3 (a) H and (b) N path flux analysis in a 0.9 N_2/0.1 H_2 AC plasma discharge at 20 kHz and 18 kV. For H and N radicals, the percentages indicate the contributions accounting for the total production and consumption. For the other species, the percentages indicate the contributions accounting for its total consumption. All percentages do not exactly sum to 100% due to minor contributions from some reactions. Purple arrow: reactions involving electron and excited species; red arrow: reactions involving ground states.

To understand the vibrational energy transfer and the subsequent N/H production, the path flux analysis of $H_2(v=1\text{-}3)$ is presented in Figure 4. The vibrational energy transfer from the high vibrational levels $N_2(v=2\text{-}8)$ to $H_2(v=1)$ is the dominant mechanism for the $H_2(v=1)$ production via V-V' exchange. Note that $N_2(v=1)$ cannot provide sufficient energy to activate $H_2(v=1)$, whereas it is primarily quenched via V-T relaxation by H_2/H/NH_3. Then the vibrational energy transfers from $H_2(v=1)$ to a higher vibrational level $H_2(v=2)$ via V-V exchange with $H_2(v=1)$ and V-V' exchange with $N_2(v=2\text{-}8)$, accounting for 5.8% and 4.5% of its total consumption respectively. Although 89% of $H_2(v=1)$ converts back to H_2 via V-V' exchange with $N_2(v=0\text{-}7)$, a considerable amount of $H_2(v=2)$ is still generated due to the large in- and out-flux of $H_2(v=1)$. The vibrational level $H_2(v=2)$ contains a higher energy that can overcome the activation energy barrier of reaction $N + H_2 = NH + H$. Figure 4 shows that 18.7% of $H_2(v=2)$ is consumed by $N + H_2(v=2) \rightarrow NH + H$, accelerating the NH and H production. Similar to the vibrational energy transfer of $H_2(v=1)$, the vibrational energy of $H_2(v=2)$ also transfers to $H_2(v=3)$ or converts back to a lower vibrational level $H_2(v=1)$. With a high vibrational energy level, 80.5% of $H_2(v=3)$ is consumed by $N + H_2(v=3) \rightarrow NH + H$. However, due to its low concentration, the $H_2(v=3)$ contribution to the NH and H production is not as high as that from $H_2(v=2)$, as shown in Figure 3. It can be concluded that vibrational energy transfer to the higher vibrational level $H_2(v=2\text{-}3)$ via the V-V exchange ($H_2(v)$-

$H_2(v)$) and V-V' exchange ($N_2(v)$-$H_2(v)$) significantly enhances the NH and H production, which further promotes the coupling between N and NH for the following NH_3 synthesis both on the catalyst surface and in the gas phase.

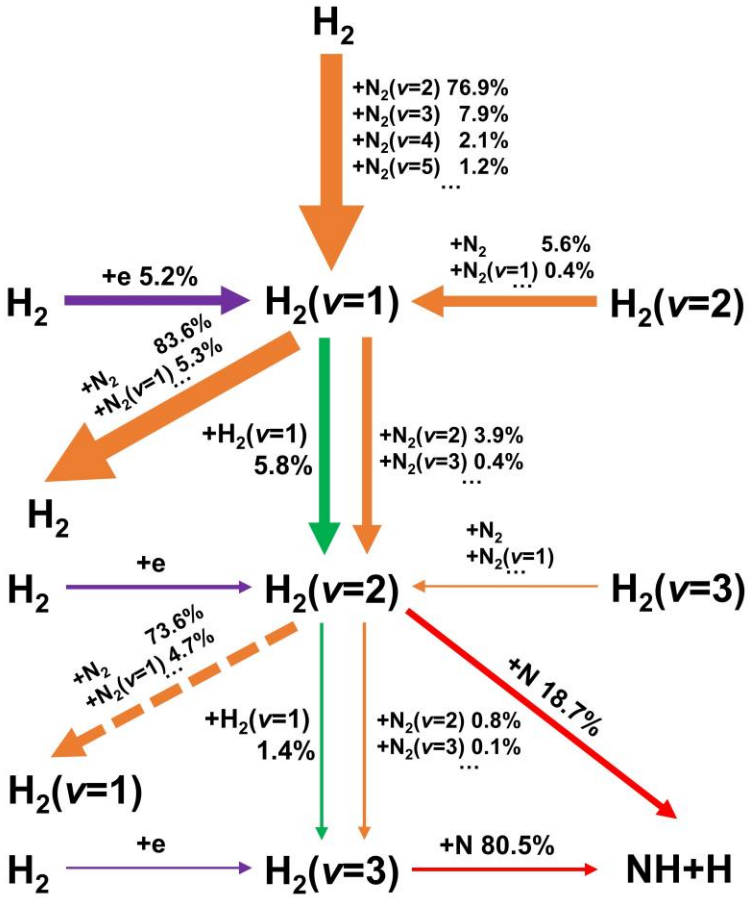

Figure 4 Vibrational energy transfer to different vibrational levels $H_2(v=1\text{-}3)$ in a 0.9 N_2/0.1H_2 AC plasma discharge at 20 kHz and 18 kV. For the $H_2(v=1)$, the percentages indicate the contributions accounting for the total production and consumption. For the other species, the percentages indicate the contributions accounting for its total consumption. All percentages do not exactly sum to 100% due to minor contributions from some reactions. The dashed line indicates the same reaction pathway. Purple arrow: electron impact excitation; orange arrow: $N_2(v)$-$H_2(v)$ (V-V') exchange; green arrow: $H_2(v)$- $H_2(v)$ (V-V) exchange; red arrow: abstraction reaction.

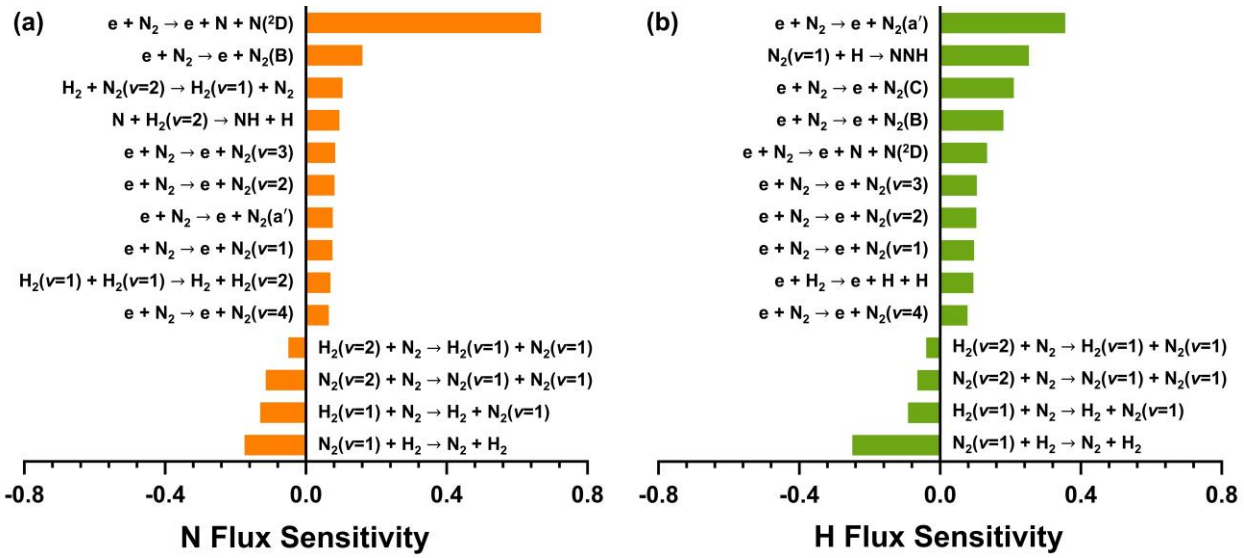

Figure 5 Sensitivity coefficients of the elementary reactions involving electrons and excited species for (a) N and (b) H production fluxes in a 0.9 N_2/0.1H_2 AC plasma discharge at 20 kHz and 18 kV.

To provide further insights into the key reaction pathways on the N and H production, the sensitivity coefficients for N and H production fluxes involving electron and excited species were calculated. A positive sensitivity coefficient indicates a promotive effect on N and H production fluxes, and vice versa. Besides the direct impact of N_2 dissociation, Figure 5(a) shows that both the production of vibrationally excited $N_2(v)$ and its vibrational energy transfer to $H_2(v)$ promote the N flux due to the enhanced coupling between N and NH. This further confirms the acceleration of the NH and H production via N + $H_2(v=2)$ → NH + H. Meanwhile, the electronically excited N_2^*, featuring large sensitivities on the H production via N_2^* + H_2 → N_2 + H + H, also contributes to the N flux as discussed in Figure 3. Figure 5(a) and (b) (the bottom four reactions) both illustrate that the reactions of V-T relaxation of $N_2(v=1)$, V-V energy transfer from $N_2(v=2)$ to $N_2(v=1)$, and V-V' energy transfer from $H_2(v=1,2)$ to $N_2(v=1)$ show the significant inhibition effects on N and H production fluxes due to the decreased $H_2(v)$ production. This confirms the kinetic roles of $H_2(v)$

in N and H production fluxes, which in turn will affect both the surface and gas-phase NH_3 production.

In summary, this work reports the non-equilibrium generation mechanism of atomic nitrogen and hydrogen to unveil the kinetic role of vibrational energy transfer in AC plasma aided ammonia synthesis. The non-equilibrium production of H and N radicals was examined using two-photon absorption laser induced fluorescence and plasma kinetic modeling. The results show that low temperature plasma generates ammonia primarily by producing critical H, N and NH radicals through both electron impact and vibrational energy transfer excitations. The vibrational energy transfer from $H_2(v=1)$ to the higher vibrational levels $H_2(v=2\text{-}3)$ via the V-V exchange ($H_2(v)$-$H_2(v)$) and V-V' exchange ($N_2(v)$-$H_2(v)$) considerably improves the production of H and NH, and then promotes the conversion between N and NH, two key intermediates for the NH_3 production both on the catalyst surface and in the gas phase.

ASSOCIATED CONTENT

Supporting Information

Supporting Information Available <Detailed experimental and numerical methods; model validation; supplementary figures; plasma aided ammonia synthesis mechanisms>

AUTHOR INFORMATION

Corresponding Author

Xingqian Mao - *Department of Mechanical and Aerospace Engineering, Princeton University, Princeton, NJ 08544, USA*; Email: xingqian@princeton.edu

Authors

Ning Liu - *Department of Mechanical and Aerospace Engineering, Princeton University, Princeton, NJ 08544, USA*

Christopher Kondratowicz - *Department of Mechanical and Aerospace Engineering, Princeton University, Princeton, NJ 08544, USA*

Timothy Y. Chen - *Department of Mechanical and Aerospace Engineering, Princeton University, Princeton, NJ 08544, USA*

Bowen Mei - *Department of Mechanical and Aerospace Engineering, Princeton University, Princeton, NJ 08544, USA*

Ziyu Wang - *Department of Mechanical and Aerospace Engineering, Princeton University, Princeton, NJ 08544, USA*

Yijie Xu - *Department of Mechanical and Aerospace Engineering, Princeton University, Princeton, NJ 08544, USA*

Hongtao Zhong - *Department of Mechanical and Aerospace Engineering, Princeton University, Princeton, NJ 08544, USA*

Zhiyu Shi - *Department of Mechanical and Aerospace Engineering, Princeton University, Princeton, NJ 08544, USA*

Anatoli Morozov - *Department of Mechanical and Aerospace Engineering, Princeton University, Princeton, NJ 08544, USA*

Arthur Dogariu - *Department of Aerospace Engineering, Texas A&M University, College Station, Texas 77843, USA*; *Department of Mechanical and Aerospace Engineering, Princeton University, Princeton, NJ 08544, USA*

Yiguang Ju - *Department of Mechanical and Aerospace Engineering, Princeton University, Princeton, NJ 08544, USA; Princeton Plasma Physics Laboratory, Princeton, NJ, USA*

ACKNOWLEDGEMENTS

This work was funded by the DOE Plasma Science Center grant DE-SC0020233, DOE BES EERC grant: DE-AC0209CH11466, and NSF grant EFMA 2029425.

Present addresses:

[#]T.Y.C.: Applied Materials, Santa Clara, CA 95054, USA

[$]H.Z.: Department of Mechanical Engineering, Stanford University, Stanford, CA 94305, USA

REFERENCES

1. Valera-Medina, A.; Xiao, H.; Owen-Jones, M.; David, W. I.; Bowen, P., Ammonia for power. *Prog. Energy Combust. Sci.* **2018,** *69*, 63-102.
2. Zhao, Y.; Wang, T.; Setzler, B. P.; Abbasi, R.; Wang, J.; Yan, Y., A high-performance gas-fed direct ammonia hydroxide exchange membrane fuel cell. *ACS Energy Lett.* **2021,** *6* (5), 1996-2002.
3. Chang, F.; Gao, W.; Guo, J.; Chen, P., Emerging materials and methods toward ammonia‐based energy storage and conversion. *Adv. Mater.* **2021,** *33* (50), 2005721.
4. Wu, S.; Salmon, N.; Li, M. M.-J.; Bañares-Alcántara, R.; Tsang, S. C. E., Energy decarbonization via green H2 or NH3? *ACS Energy Lett.* **2022,** *7* (3), 1021-1033.
5. Guo, F.; Li, C.; Xiu, X.; Cheng, K.; Qin, J., Comprehensive technical analyses of a solid oxide fuel cell turbine-less hybrid aircraft propulsion system using ammonia and methane as alternative fuels. *Appl. Therm. Eng.* **2023,** *230*, 120787.
6. Lim, J.; Fernández, C. A.; Lee, S. W.; Hatzell, M. C., Ammonia and nitric acid demands for fertilizer use in 2050. *ACS Energy Lett.* **2021,** *6* (10), 3676-3685.

7. Lhuillier, C.; Brequigny, P.; Contino, F.; Mounaïm-Rousselle, C., Experimental study on ammonia/hydrogen/air combustion in spark ignition engine conditions. *Fuel* **2020,** *269*, 117448.
8. Boretti, A.; Castelletto, S., NH3 prospects in combustion engines and fuel cells for commercial aviation by 2030. *ACS Energy Lett.* **2022,** *7* (8), 2557-2564.
9. Smith, C.; Hill, A. K.; Torrente-Murciano, L., Current and future role of Haber–Bosch ammonia in a carbon-free energy landscape. *Energy Environ. Sci.* **2020,** *13* (2), 331-344.
10. Lee, B.; Winter, L. R.; Lee, H.; Lim, D.; Lim, H.; Elimelech, M., Pathways to a Green Ammonia Future. *ACS Energy Lett.* **2022,** *7* (9), 3032-3038.
11. van 't Veer, K.; Engelmann, Y.; Reniers, F.; Bogaerts, A., Plasma-catalytic ammonia synthesis in a DBD plasma: role of microdischarges and their afterglows. *J. Phys. Chem. C* **2020,** *124* (42), 22871-22883.
12. Zhao, H.; Song, G.; Chen, Z.; Yang, X.; Yan, C.; Abe, S.; Ju, Y.; Sundaresan, S.; Koel, B. E., In situ identification of NNH and N2H2 by using molecular-beam mass spectrometry in plasma-assisted catalysis for NH3 synthesis. *ACS Energy Lett.* **2021,** *7* (1), 53-58.
13. Liu, T.-W.; Gorky, F.; Carreon, M. L.; Gómez-Gualdrón, D. A., Energetics of reaction pathways enabled by N and H radicals during catalytic, plasma-assisted NH3 synthesis. *ACS Sustain. Chem. Eng.* **2022,** *10* (6), 2034-2051.
14. Mehta, P.; Barboun, P.; Herrera, F. A.; Kim, J.; Rumbach, P.; Go, D. B.; Hicks, J. C.; Schneider, W. F., Overcoming ammonia synthesis scaling relations with plasma-enabled catalysis. *Nat. Catal.* **2018,** *1* (4), 269-275.
15. Bayer, B. N.; Bruggeman, P. J.; Bhan, A., Species, Pathways, and Timescales for NH3 Formation by Low-Temperature Atmospheric Pressure Plasma Catalysis. *ACS Catal.* **2023,** *13* (4), 2619-2630.
16. Yang, X.; Jans, E.; Richards, C.; Raskar, S.; van den Bekerom, D.; Wu, K.; Adamovich, I. V., Measurements of atoms and metastable species in N2 and H2–N2 nanosecond pulse plasmas. *Plasma Sources Sci. Technol.* **2022,** *31* (1), 015017.
17. Wang, Y.; Craven, M.; Yu, X.; Ding, J.; Bryant, P.; Huang, J.; Tu, X., Plasma-enhanced catalytic synthesis of ammonia over a Ni/Al2O3 catalyst at near-room temperature: insights into the importance of the catalyst surface on the reaction mechanism. *ACS catal.* **2019,** *9* (12), 10780-10793.

18. Liu, N.; Chen, T.; Zhong, H.; Kondratowicz, C.; Ju, Y. In *Quantitative femtosecond two-photon absorption laser induced fluorescence measurements of hydrogen and nitrogen atoms in an AC dielectric barrier discharge*, AIAA SCITECH 2023 Forum, 2023; p 0351.
19. Liu, N.; Zhong, H.; Chen, T. Y.; Lin, Y.; Wang, Z.; Ju, Y., Sensitive and single-shot OH and temperature measurements by femtosecond cavity-enhanced absorption spectroscopy. *Opt. Lett.* **2022,** *47* (13), 3171-3174.
20. Liu, N.; Chen, T. Y.; Zhong, H.; Lin, Y.; Wang, Z.; Ju, Y., Femtosecond ultraviolet laser absorption spectroscopy for simultaneous measurements of temperature and OH concentration. *Appl. Phys. Lett.* **2022,** *120* (20), 201103.
21. Chen, T. Y.; Liu, N.; Kliewer, C. J.; Dogariu, A.; Kolemen, E.; Ju, Y., Simultaneous single-shot rotation–vibration non-equilibrium thermometry using pure rotational fs/ps CARS coherence beating. *Opt. Lett.* **2022,** *47* (6), 1351-1354.
22. Niemi, K.; Schulz-Von Der Gathen, V.; Döbele, H., Absolute calibration of atomic density measurements by laser-induced fluorescence spectroscopy with two-photon excitation. *J. Phys. D: Appl. Phys.* **2001,** *34* (15), 2330.
23. Dumitrache, C.; Gallant, A.; de Oliveira, N.; Laux, C. O.; Stancu, G. D., Quantitative fs-TALIF in high-pressure NRP discharges: calibration using VUV absorption spectroscopy. *Plasma Sources Sci. Technol.* **2022,** *31* (1), 015004.
24. Urdaneta, G.; Uddi, M.; Kudlanov, E.; Dogariu, A. In *Fs-TALIF for Low Pressure Interfacial Plasmas*, AIAA SCITECH 2024 Forum, 2024; p 0805.
25. Miles, R.; Dogariu, A.; Dogariu, L., Localized time accurate sampling of nonequilibrium and unsteady hypersonic flows: methods and horizons. *Exp. Fluids* **2021,** *62* (12), 248.
26. Dogariu, A.; Evans, E.; Vinoth, S.; Cohen, S. In *Neutral Atomic-Hydrogen Measurements in a Mirror/FRC Plasma Device using fs-TALIF*, APS Annual Gaseous Electronics Meeting Abstracts, 2020; p JT2. 005.
27. Mao, X.; Rousso, A.; Chen, Q.; Ju, Y., Numerical modeling of ignition enhancement of CH4/O2/He mixtures using a hybrid repetitive nanosecond and DC discharge. *Proc. Combust. Inst.* **2019,** *37* (4), 5545-5552.
28. Mao, X.; Chen, Q.; Rousso, A. C.; Chen, T. Y.; Ju, Y., Effects of controlled non-equilibrium excitation on H2/O2/He ignition using a hybrid repetitive nanosecond and DC discharge. *Combust. Flame* **2019,** *206*, 522-535.

29. Gou, X.; Sun, W.; Chen, Z.; Ju, Y., A dynamic multi-timescale method for combustion modeling with detailed and reduced chemical kinetic mechanisms. *Combust. Flame* **2010,** *157* (6), 1111-1121.
30. Mao, X.; Zhong, H.; Zhang, T.; Starikovskiy, A.; Ju, Y., Modeling of the effects of non-equilibrium excitation and electrode geometry on H2/air ignition in a nanosecond plasma discharge. *Combust. Flame* **2022,** *240*, 112046.
31. Zhong, H.; Mao, X.; Liu, N.; Wang, Z.; Ombrello, T.; Ju, Y., Understanding non-equilibrium N2O/NOx chemistry in plasma-assisted low-temperature NH3 oxidation. *Combust. Flame* **2023,** *256*, 112948.
32. Mao, X.; Zhong, H.; Liu, N.; Wang, Z.; Ju, Y., Ignition enhancement and NOx formation of NH3/air mixtures by non-equilibrium plasma discharge. *Combust. Flame* **2024,** *259*, 113140.
33. Capitelli, M.; Ferreira, C. M.; Gordiets, B. F.; Osipov, A. I., *Plasma kinetics in atmospheric gases*. Springer Science & Business Media: 2013; Vol. 31.
34. Fridman, A., *Plasma chemistry*. Cambridge university press: 2008.